ADVANCED ENERGY MATERIALS
www.advenergymat.de

Highly Integrated Triboelectric-Electromagnetic Wave Energy Harvester toward Self-Powered Marine Buoy

Chuanqing Zhu, Mengwei Wu, Chang Liu, Cheng Xiang, Ruijiang Xu, Hengyi Yang, Zhaoyang Wang, Ziyu Wang, Peng Xu, Fuzhen Xing, Hao Wang, and Minyi Xu**

This paper proposes a highly integrated triboelectric-electromagnetic wave energy harvester (TEWEH) that can efficiently collect wide-frequency wave energy and realize a self-powered marine buoy. The innovative design of a permanent magnet-polytetrafluoroethylene (PM-PTFE) ball ensures high integration between the magnetic material forming the electromagnetic generator (EMG) and the dielectric material forming the triboelectric nanogenerator (TENG). In the condition of swinging (1 Hz and ±30°), the output of the TENG component can reach 230.25 V, 1.34 µA, and the average output of the EMG is 2.30 V, 10.43 mA. Remarkably, even at an extremely low frequency (0.2 Hz), the TEWEH maintains exceptional output. The output power density of the TENG component and EMG component reach 13.77 W m^{-3} and 148.24 W m^{-3}, respectively, which are much higher than in previous work. The TEWEH can quickly charge the 330 µF capacitor to a certain voltage, and then light up navigation mark lights and power thermometers. A sealed TEWEH with circuits works as a self-powered marine buoy that can transmit actual marine ambient temperatures to land. In conclusion, the TEWEH has broad application prospects in the field of wave energy harvesting and the self-powered marine Internet of Things.

1. Introduction

Oceans are abundant sources of renewable energy,[1] such as tidal energy,[2] current energy,[3] and wave energy.[4,5] Wave energy holds great promise as an energy resource because of its high energy density and accessibility.[6,7] Researchers are actively developing wave energy technology and expecting it to power distributed marine devices such as the marine Internet of Things (MIoT). Electromagnetic generators (EMGs) are the primary means for harvesting wave energy.[8–12] However, most EMGs have complex structures, making their integration with small-scale sensors less desirable.[13,14] In addition, the low frequency of ocean waves and sometimes low-amplitude characteristics are not favorable for EMGs (to operate efficiently) and should be supplemented by other alternatives.

The triboelectric nanogenerator (TENG), invented by Wang et al. in 2012, can effectively harvest mechanical energy from the environment.[15] It has been widely studied for harvesting wind,[16–19] vibration,[20–22] and wave energies.[23–27] Zi et al. have systematically compared the output performance of the EMG and the TENG with low-frequency input.[28] The power density of the EMG is proportional to the square of the frequency, whereas the power density of the TENG is proportional to the frequency, indicating that the TENG is more effective in harvesting low-frequency mechanical energy, such as wave energy. Considering TENG's advantages of the TENG material composition (mostly anticorrosive), good robustness, and low cost, it has the potential to be an appropriate generator for various marine sensors and buoys.

On observing the output characteristics of the EMG (low voltage and high current) and TENG (high voltage and low current), as well as their preference in the operating conditions, the idea of triboelectric-electromagnetic harvesters with both EMG and TENG integrated is proposed.[29–33] This idea not only expands the frequency range of energy harvesting, but also improves the energy harvesting efficiency. In recent years, various triboelectric-electromagnetic harvesters have been proposed and studied.[34–40] Most studies have constructed the EMG and the TENG separately and then attached them together. The designs also reduce the output of both power generation modes and in many cases significantly increase the generator volume. Liao et al. developed a cubic-structure harvester by integrating the TENG and the EMG together, which can improve the overall output performance by reducing the volume through an optimized inner topological structure.[41] Xu et al. arranged the moving parts of the EMG and the TENG onto the same rotor, which could simultaneously output under wave excitation.[42] Yang et al. placed deionized water and a magnet in a tube that can oscillate

C. Zhu, C. Liu, C. Xiang, R. Xu, H. Yang, Z. Wang, Z. Wang, P. Xu, F. Xing, H. Wang, M. Xu
Dalian Key Lab of Marine Micro/Nano Energy and Self-powered System
Marine Engineering College
Dalian Maritime University
Dalian 116026, China
E-mail: hao8901@dlmu.edu.cn; xuminyi@dlmu.edu.cn
M. Wu
College of Engineering
Peking University
Beijing 100871, China

The ORCID identification number(s) for the author(s) of this article can be found under https://doi.org/10.1002/aenm.202301665

DOI: 10.1002/aenm.202301665

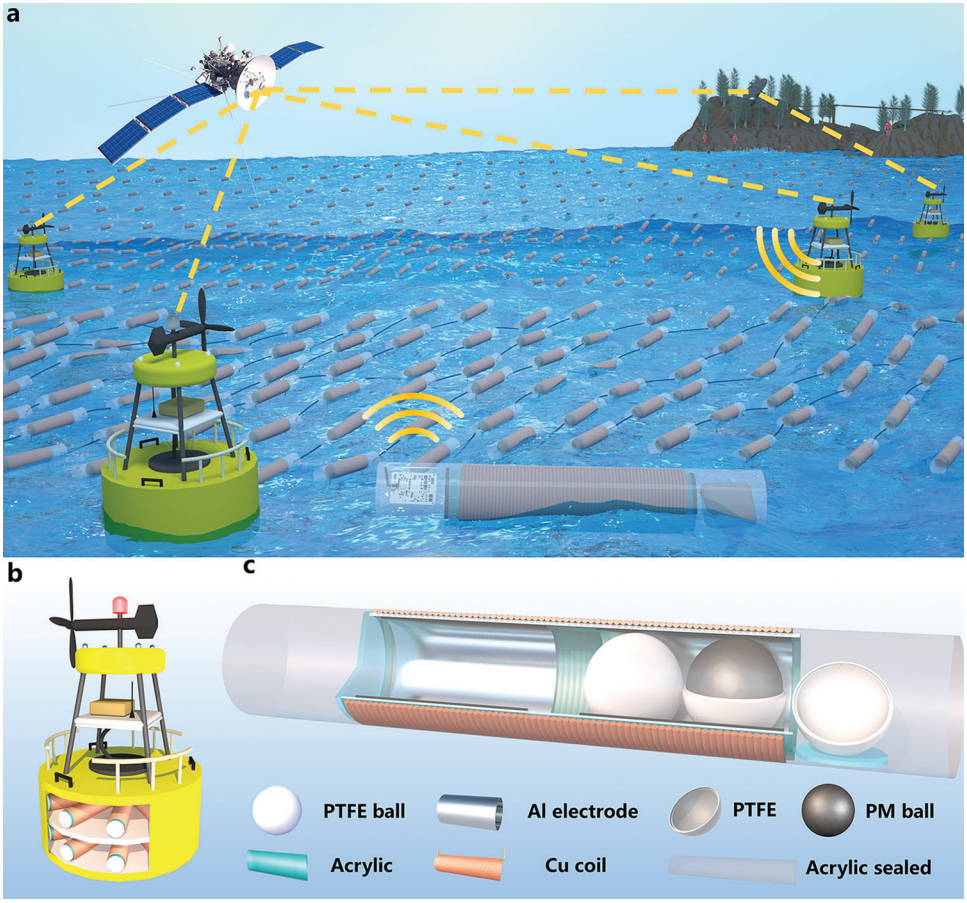

Figure 1. Application scenario and structure diagram of the TEWEH. a) Schematic of the TEWEH applied in wave energy harvesting and self-powered MIoT. b) Schematic of the TEWEH integrated inside a buoy as the power supply. c) The internal view of the TEWEH's structure.

under wave excitations, and the fluidity of the fluid effectively reduces the structural volume; however, there is still a problem with the low utilization rate of the liquid placement space.[43] It is worth noting that the presence of TENG structures in these studies still created significant gaps between the magnets and coils in the EMG, greatly affecting the output performance of the EMG. Kim et al. designed a hybrid generator with a tubular structure and innovatively arranged the TENG inside the EMG to reduce the volume and gap. However, the sliding friction of the internal cylindrical magnet challenged its durability, and the EMG could not output at low frequencies (<1.5 Hz).[44] Therefore, it is critical to fully integrate the TENG and EMG power generation components and enable them to move effectively under low-frequency wave excitation to achieve an efficient dual-mode output in the same volume unit and to reduce or even avoid negative impacts on each other.

Herein, we propose a highly integrated triboelectric-electromagnetic wave energy harvester (TEWEH) that can harvest wave energy under a wide frequency range and arbitrary wave excitations. A TEWEH embeds a permanent magnet (PM) ball into a polytetrafluoroethylene (PTFE) shell to form a permanent magnet-polytetrafluoroethylene (PM-PTFE) ball, which efficiently utilizes the space of the wave energy harvester and significantly improves the output power density. As the PM-PTFE ball moved, the TENG and EMG components simultaneously generated electricity. The instability of the ball motion allows the TEWEH to harvest wave energy of ultra-low-frequency and extremely small amplitude. The output performance of the TEWEH's TENG component and its EMG component were systematically analyzed, and the power density was found to be higher than that of previous harvesters.[41,45–49] With appropriate circuit management, the output of the TEWEH fully demonstrates the advantages of combining the TENG component and EMG component. In water tank testing, the TEWEH yields a desirable output and easily powers common marine devices such as navigation lights and thermometers. Finally, the TEWEH demonstrated its capability to collect actual ocean temperature data and transmit it to a receiver on land. Hence, the TEWEH has broad application prospects in marine monitoring, navigation support, and marine exploitation.

2. Results and Discussion

2.1. Configuration and Working Principle of the TEWEH

Figure 1a shows a schematic of the TEWEH utilized for wave energy harvesting and self-powered MIoT. The TEWEH can be deployed extensively on the ocean in a grid-scale configuration. The

harvested wave energy can power outlying islands or be transferred to a land grid. The appropriate number of TEWEHs on each platform was determined based on the demands of the actual marine equipment. A self-powered MIoT can be achieved by matching the TEWEH with the demand. Most importantly, the sealed TEWEH could be independently placed on the sea surface to function as a self-powered marine buoy. A photograph of the single sealed TEWEH is presented in Figure S1a (Supporting Information). The ends of the acrylic-sealed cabin were extended to promote the stability of the TEWEH, in case it overturns due to the rolling ball. The remaining space can accommodate the placement of the sensors and circuits. This type of buoy has the advantages of a simple structure, easy deployment, and strong adaptability. The collected marine information can be received through satellites or land-based radars.

The integration of the TEWEH as a power supply inside the buoy is shown in Figure 1b. Because of the presence of magnetic balls within the TEWEH, mutual attraction or repulsion can influence the output. Therefore, the TEWEHs were arranged at appropriate distances between them. Figure 1c shows an internal view of the TEWEH structure. The customized acrylic tube had an inner diameter of 31 mm and an outer diameter of 35 mm. Aluminum (Al) electrodes were attached to the inner perimeter, whereas copper (Cu) wire coils were wrapped around the outer perimeter. The ends of the coil served as output sites for EMG.

The effect of coil turns on the output of the EMG component is shown in Figure S2 (Supporting Information). The voltage increased with the number of turns in the coil (a change in the number of layers corresponds to a change in the number of turns), but the current yielded the opposite tendency. While securing the output voltage, the output current should be as large as possible; therefore, we wrapped three layers of coils outside the tube. The Al electrode features a 10 mm gap in the middle, dividing it into left and right segments. The left and right segments of the Al electrode were connected to the Cu wires, respectively, as the output sites of the TENG. The PM-PTFE ball was formed by embedding a 25 mm PM ball into a PTFE ball shell with an inner diameter of 25 mm. The details of the PM-PTFE ball can be seen in Figure S1b (Supporting Information). The remanence of the PM-PTFE ball was measured using a Gauss meter.

The innovative design of the PM-PTFE ball ensured high integration between the magnetic material forming the EMG and the dielectric material forming the TENG. At the same time, this design reduces the volume of the entire harvester, thereby enhancing the output power density. Because the TEWEH is excited by waves, both the TENG and EMG operate simultaneously. Acting as the moving part of the TEWEH, the ball (with its center of gravity positioned at its geometric center) can move in wide-frequency and arbitrary wave excitations, enhancing the adaptability of the TEWEH to the marine environment.

The power-generation processes of the TENG and EMG components in a TEWEH are independent of each other. Therefore, they were analyzed separately. The working principle of the TENG component is shown in four continuous steps in **Figure 2**a, in which only the PTFE ball is drawn to clearly demonstrate the process of power generation. Owing to the wave excitation, the ball moved back and forth within the tube, while the PTFE ball repeatedly made contact and separated from the Al electrodes (left and right). Because of the difference in the triboelectric charging affinity between PTFE and Al, when the PTFE ball is in the position depicted in Figure 2a(i), it is negatively charged, whereas the left Al electrode in contact with PTFE is positively charged (with the same amount of charge). When the PTFE ball moved to the position shown in Figure 2a(ii), it retained a significant amount of negative charge because of the electret nature of PTFE. Upon contact between the PTFE ball and the right Al electrode, electrons are transferred from the right electrode to the left electrode through the external circuit, balancing the potential difference with the ball and generating the current from left to right. When the PTFE ball was situated as depicted in Figure 2a(iii), the right electrode accumulated the same amount of positive charge as the negative charge carried by the ball. Similarly, as shown in Figure 2a(iv), when the ball moved to the left under wave excitation, an external current was generated from right to left. In actual cycles, the ball continuously moves back and forth, resulting in the production of an alternating current (AC) output in the external circuit. The potential difference between the TENG electrodes was simulated using the COMSOL software and is presented in Figure 2b(i–iv). This provides a clear visualization of the potential difference that drives the current between the electrodes.

The TENG component in the TEWEH can be classified under the freestanding triboelectric-layer mode, therefore its output voltage (E_t) can be described by Equation (1):

$$E_t = -\frac{1}{C}Q + V_{oc} \tag{1}$$

Q, C, and V_{oc} represent the total transferred charge, capacitance, and open-circuit voltage, respectively.

The working principle of the EMG component is illustrated in four consecutive steps in Figure 2c. Similarly, only the PM-PTFE ball is drawn in this section. In the figure, the PM ball is simplified as a bar magnet. As shown in Figure 2c(i–ii), upon wave excitation, the PM-PTFE ball initiated a rolling movement from left to right. As the PM-PTFE ball initiates its rolling movement, the accompanying magnetic field begins to rotate and intersect the coil, thus generating an induced current. As indicated in Figure 2c(iii–iv), when the rotation of the PM-PTFE ball exceeded 90°, opposing induced currents were produced within the coil. Given that certain coil wires generate current while the remaining parts serve as random loads, coil selection is critical. The corresponding magnetic field distributions at various PM-PTFE ball positions were simulated using COMSOL, as shown in Figure 2d(i–iv).

According to Faraday's law of electromagnetic induction and Ohm's law, the output voltage (E_e) and current (I) of the EMG can be determined using Equations (2)–(5):

$$E_e = -n\frac{\Delta \Phi}{\Delta t} = -nBlv' \tag{2}$$

$$v' = v\cos\theta_1\cos 2\theta_2 \tag{3}$$

$$E_e = -nBlv\cos\theta_1\cos 2\theta_2 \tag{4}$$

$$I = \frac{E_e}{R_c} = \frac{-nBlv\cos\theta_1\cos 2\theta_2}{R_c} \tag{5}$$

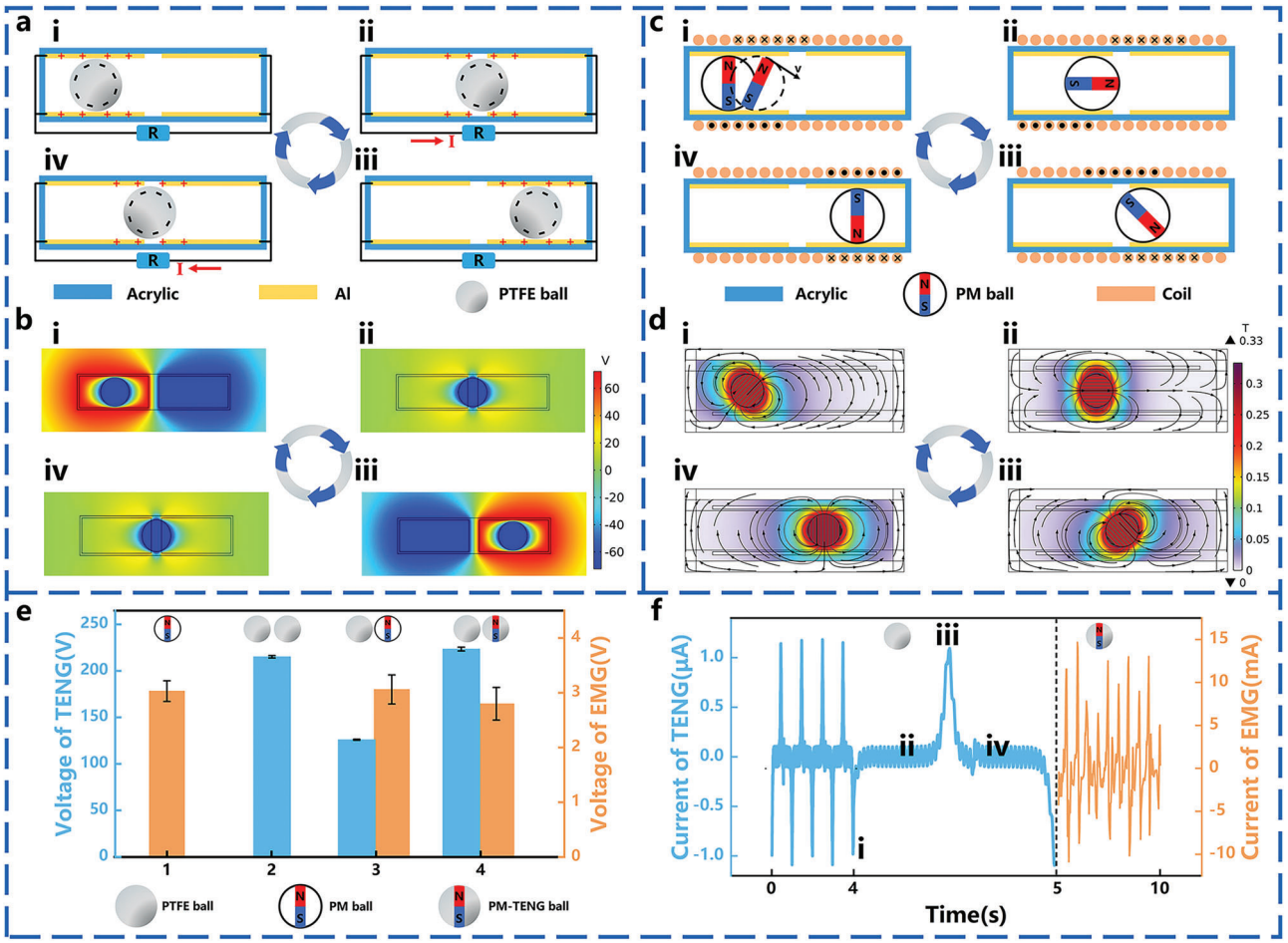

Figure 2. The working principle and output characteristics of the TEWEH. a) Schematic of the TENG component's working principle. b) Simulation of the potential difference across the electrodes under open-circuit conditions using COMSOL. c) Schematic of the EMG component's working principle. d) Simulation of the magnetic field distribution around the PM-PTFE ball using COMSOL. e) The output voltage with various ball types. f) Real-time current output of the TENG component and the EMG component.

where n, Φ, B, l, and R_c represent the number of turns, magnetic flux, magnetic induction intensity, effective length of the coil and internal resistance of the coil. The v and v' represent the velocity of the PM-PTFE ball and the tangential velocity of the PM-PTFE ball as it rotates, respectively. Furthermore, θ_1 signifies the rotational angle of the ball and θ_2 is the deflection angle of the ball, as shown in Figure S3 (Supporting Information).

To determine the effect of structural design on output performance, various types of balls were tested in the tube under wave-swinging conditions of 1 Hz and ±30°. As shown in Figure 2e, when a single magnet ball was placed in the tube, the average output voltage of the EMG was ≈3.03 V. Incorporating a PTFE ball did not notably influence the EMG output, yet it resulted in a high voltage of 125.88 V from the TENG. When the PM-PTFE ball and PTFE ball were implemented (as the final design of the TEWEH), the EMG output exhibited a minor decrease, but the TENG output voltage significantly increased to 223.37 V. This outcome can be attributed to the greater weight of the PM-PTFE ball compared to that of the PTFE ball, thereby increasing the surface friction. The voltage output of the TENG significantly surpassed that of the EMG. Thus, it is reasonable to achieve a high-voltage output from the TENG at the expense of a less than 1 V reduction in the EMG output. Figure 2f shows the actual output current waveforms of the TENG and the EMG. The current from the EMG was significantly higher than that from the TENG, highlighting the necessity of EMG.

The TENG output exhibited a close correlation with the schematic depicted in Figure 2a(i–iv), whereas the EMG output displayed fluctuations. Due to the different masses of the two balls and placed in front and back, they come into contact with the other electrode one after another, resulting in no current change during this period in Process II. The motion of the ball, with its surface marked for enhanced observation of movement within the tube, was captured using a high-speed camera. In this particular scenario, for clearer observation, the acrylic tube was devoid of electrodes and coils. As shown in Video S1 (Supporting Information), the motion process aligns with the working principle diagram. In addition to rolling, the balls vibrated when in contact with the tube wall. This phenomenon, combined with the ball deflection angle θ_2 mentioned in Equation (5), results in irregular variations in the magnetic field and, consequently, an irregular EMG output. Therefore, for a streamlined analysis and

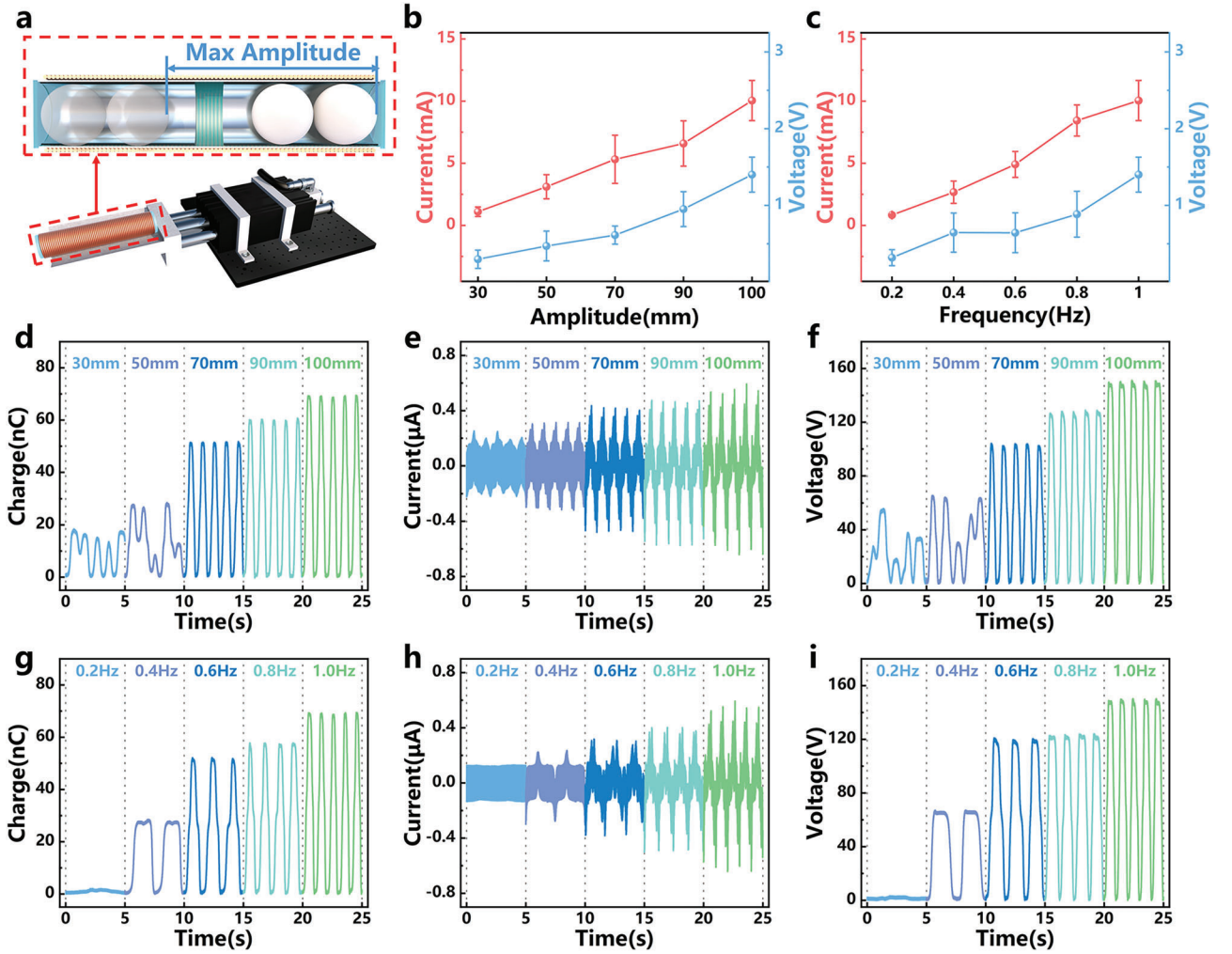

Figure 3. The output performance of the TEWEH under horizontal excitation. a) Schematic of the horizontal excitation experiment system. b) $|V_{avg}|$ and $|I_{avg}|$ for the EMG component under different amplitudes at the frequency of 1 Hz. c) $|V_{avg}|$ and $|I_{avg}|$ for the EMG component under different frequencies at the amplitude of 100 mm. d) Q_{sc}, e) I_{sc}, and f) V_{oc} for the TENG component under different amplitude at the frequency of 1 Hz. g) Q_{sc}, h) I_{sc}, and i) V_{oc} for the TENG component under different frequencies at the amplitude of 100 mm.

comparison, the EMG output in the subsequent discussion utilized the average value. Nonetheless, this has no impact on wave energy harvesting, as both the TENG and EMG outputs are subject to rectification for applications.

2.2. Performance of the TEWEH

To evaluate the output performance of the TEWEH, an experimental system was constructed to simulate horizontal wave excitation. As depicted in **Figure 3**a, the system primarily comprises a linear motor and a testing platform affixed to the front of the motor. A photograph of the system is presented in Figure S4a (Supporting Information). The TEWEH was secured on a testing platform to ensure an interference-free magnetic field, with the linear motor generating a horizontal reciprocating motion with adjustable frequency and amplitude. Initially, the influence of the frequency and amplitude on the EMG average output voltage ($|V_{avg}|$) and current ($|I_{avg}|$) was investigated. At the frequency of 1 Hz, when the amplitude incrementally increased from 30 to 100 mm, the $|V_{avg}|$ of the EMG escalated from 0.30 to 1.40 V, and the $|I_{avg}|$ rose from 1.10 to 10.04 mA. Upon maintaining the amplitude at 100 mm and increasing the frequency from 0.2 to 1 Hz, the $|V_{avg}|$ of the EMG increased from 0.32 to 1.40 V, and the $|I_{avg}|$ amplified from 0.83 to 10.04 mA. An important finding is that the changes in $|V_{avg}|$ and $|I_{avg}|$ of the EMG are not proportional, as this ratio represents the internal resistance of the EMG, which constantly changes with the movement of the PM-PTFE ball. This is because the structural resistance of the coil is constantly changing with the ball's movement, and is also affected by the inductance of the coil.

The variations in the transfer charge (Q_{sc}), short-circuit current (I_{sc}), and open-circuit voltage (V_{oc}) of the TENG with increasing amplitude at a frequency of 1 Hz are depicted in Figure 3d–f. As shown in Figure 3a, the maximum displacement of the ball within the tube was 90 mm. Consequently, when the amplitude reached 100 mm, the output reached its apex, and Q_{sc}, I_{sc}, and V_{oc} reached 69.15 nC, 0.55 μA, and 151.20 V, respectively.

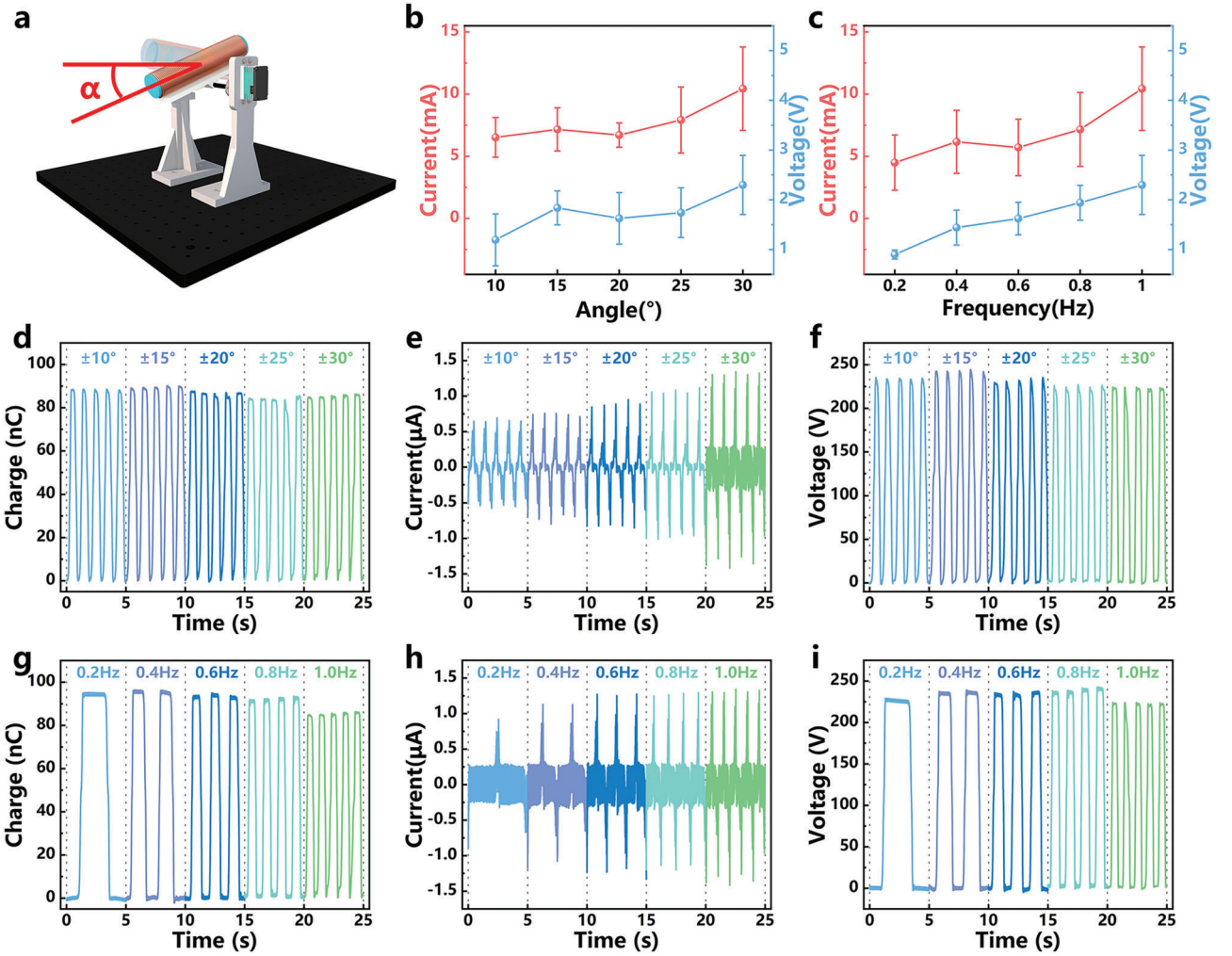

Figure 4. The output performance of the TEWEH under swinging excitation. a) Schematic of the experiment system for swinging. b) $|V_{avg}|$ and $|I_{avg}|$ for the EMG component under different angles at the frequency of 1 Hz. c) $|V_{avg}|$ and $|I_{avg}|$ for the EMG component under different frequencies at the swinging angle of ±30°. d) Q_{sc}, e) I_{sc}, and f) V_{oc} for the TENG component under different angles at the frequency of 1 Hz. g) Q_{sc}, h) I_{sc}, and i) V_{oc} for the TENG component under different frequencies at the swinging angle of ±30°.

Considering the inter-electrode distance of 70 mm at both ends, in extreme scenarios, both small balls require at least a 65 mm stroke to complete a full cycle. When the amplitude was below this value, the small ball moved back and forth several times and constantly contacted and separated the two electrodes near the midpoint to maintain stability. The experimental results corroborated this observation; the output of the TENG component was intermittent at amplitudes of 30 and 50 mm. Therefore, even at smaller wave amplitudes, the TENG can still produce effective output. Figure 3g–i illustrate the impact of frequency variations on the output performance of the TENG while maintaining a constant amplitude of 100 mm. Both Q_{sc} and V_{oc} increased less with the frequency, which is attributable to the limited area of the dielectric material, resulting in an induced charge threshold. Conversely, the I_{sc} climbed linearly with the frequency, because the increased frequency led to accelerated charge transfer. The maximum frequency was determined to be 1 Hz, considering at typical marine environment wave frequency ranges of 0.1 Hz and 1 Hz. The TENG exhibited substantial output across most frequencies within this range. The additional output performance of the TEWEH under varying amplitudes and frequencies is shown in Figure S4b–d (Supporting Information).

An experiment system was designed to evaluate the influence of varying swinging angles ($\pm\alpha$) and frequencies on the output performance of the TEWEH. **Figure 4**a presents a schematic of this system, and a corresponding photograph is shown in Figure S5a (Supporting Information). The TEWEH was affixed to the testing platform with a steering engine that supplied swinging torque via the axis system. $|V_{avg}|$ and $|I_{avg}|$ of the EMG vary with the swinging angle and frequency, as shown in Figure 4b,c, respectively. Maintaining the frequency at 1 Hz while increasing the swinging angle from ±10° to ±30° resulted in the escalation of the EMG's $|V_{avg}|$ from 1.19 to 2.30 V. Simultaneously, the $|I_{avg}|$ increased from 6.52 to 10.43 mA. Similar to the horizontal cases, amplifying the swinging frequency also enhanced the EMG output. With a swinging angle of ±30° and a frequency increment from 0.2 to 1 Hz, the EMG's $|V_{avg}|$ and $|I_{avg}|$ increased from 0.90 V and 4.49 mA to 2.30 V and 10.43 mA, respectively.

The effect of the swinging angle on the TENG output was studied by maintaining the swinging frequency at 1 Hz. As shown in Figure 4d,f, when the swinging angle spanned from ±10° to ±20°, the TENG's Q_{sc} and V_{oc} remained relatively stable at ≈88.36 nC and 230.25 V, respectively. Once the swinging angle surpassed ±25°, they experienced a slight decrease to 85.28 nC and 225.65 V, respectively. This trend can be attributed to the ball effectively completing the entire stroke in all the tested cases. The surface charge density reaches saturation, and as a result, Q_{sc} and the potential difference between the electrodes attain their maximum values and, hence, their constancy. However, once the swinging angle exceeded ±25°, it became sufficiently large to cause minor gaps between the ball and electrode, which slightly reduced Q_{sc}. This phenomenon is observed in Video S1 (Supporting Information) of the movement. As shown in Figure 4e, the I_{sc} escalated with increasing swinging angle, ranging from 0.66 μA at 0.2 Hz to 1.34 μA at 1.0 Hz. This energy originates from the ball's potential energy, which grows with the swinging angle and transforms into the ball's kinetic energy, subsequently amplifying the ball's acceleration and consequently leading to a current surge.

Furthermore, the effect of the swinging frequency on the output performance of the TENG was studied, while the swinging angle was held constant at ±30°. As shown in Figures 4g,i, the peak values of V_{oc} and Q_{sc} were relatively stable and experienced a slight decline at 1 Hz. This was also because the TEWEH could finish a complete stroke at all frequencies, whereas at 1 Hz, rapid movement may give rise to gaps (between the ball and the electrode). As shown in Figure 4h, the magnitude of I_{sc} correlates positively with the frequency, similar to the horizontal mode. Most importantly, the TENG continued to yield satisfactory output even at extremely low frequencies, such as 0.2 Hz. This also indicated that TEWEH has an advantage in wide-frequency range harvesting. Detailed output under diverse swinging angles and frequencies is presented in Figure S5b–d (Supporting Information).

Notably, the output of the TEWEH in swinging mode significantly surpasses that in horizontal mode, making it desirable for wave energy harvesting. Specifically, the EMG's maximum output escalated from 1.40 V and 10.04 mA to 2.30 V and 10.43 mA, while the TENG's maximum output rose from 69.145 nC, 0.553 μA, and 151.20 V to 88.36 nC, 1.34 μA, and 230.25 V. This performance enhancement in the swinging mode was attributable to the ball's ability to roll more fluid and swiftly, provoking rapid magnetic field variations, thereby augmenting the EMG output. This simultaneously enabled the ball to contact the electrodes in all directions, which bolstered the output of the TENG. We found that efficient integration of the TENG and EMG through the ball structure is appropriate for wave energy harvesting. The motion characteristics of the ball ensured that the TEWEH operated even under a wide frequency range and arbitrary wave excitations.

To use the TEWEH as a power source, its output power density and capacitor charging capability were tested. Utilizing the swinging experiment system under 1 Hz and ±30° conditions, the 3.3 μF capacitor has been charged using the EMG component, the TENG component, and the TEWEH, respectively. The real-time voltage change in the capacitor was recorded for over 300 s. The charging circuit is shown in Figure S6 (Supporting Information). As demonstrated in **Figure 5**a, the EMG component swiftly charged the capacitor to a certain voltage owing to its high output current, but encountered difficulties in further increasing the voltage. Conversely, the TENG component charges the capacitor at a stable rate and relatively high voltage, which is attributed to the high-voltage output characteristics of the TENG. When charging the capacitor using the TEWEH, the EMG and TENG components were rectified individually before being connected in parallel to charge the capacitor. The TEWEH combines the advantages of both generators, which not only charges the capacitor more rapidly (than the TENG-only case), but also charges the capacitor to a higher voltage (than the EMG-only case). A 3.3 μF capacitor could reach 5.74 V within 11 s and 9.41 V after 300 s. The charging process for larger capacitors, shown in Figure 5b, yielded a similar charging curve. In light of the randomness and relatively low frequency of actual ocean waves, various frequencies were tested when charging the 330 μF capacitor, as portrayed in Figure 5c. Remarkably, even at extremely low frequency (0.2 Hz), the capacitor could be charged. This again proved the advantage of the TEWEH in harvesting low-frequency wave energy.

To assess the suitability of the TEWEH as a power source for a self-powered MIoT, its output power was analyzed. The generator can achieve its maximum output by matching the impedance. As shown in Figure 5d,e, the power densities of the TENG and EMG components were measured using the swinging experiment system at 1 Hz and ±30°. The TENG component exhibited an instantaneous power density of 13.77 W m^{-3} when matched with a 9000 MΩ resistor, whereas the EMG component demonstrated an instantaneous power density of 148.24 W m^{-3} when matched with a 500 Ω resistor. Overall, the TEWEH achieved a minimum output of 162.01 W m^{-3}, which is sufficient to meet the power requirements of most current marine sensing nodes.[50]

A comparison of the output power densities of the TENG-EMG hybrid studies is shown in Figure 5f. The output power density of the TENG component in the TEWEH was significantly higher than those reported in previous studies, which could be attributed to the advantages of the channel-type ball structure.[51] This TEWEH achieved a breakthrough in the output power density of the EMG component compared with previous homogeneous harvesters. This is due to the reduced gap between the magnet and coil, allowing the coil to capture the magnetic field changes caused by any movement of the PM-PTFE ball. The high output power density of a single TEWEH makes it a more reliable power supply module and reduces the volume, deployment difficulty, and maintenance cost of wave energy harvesting. The detailed data and comparison with more state-of-the-art devices are summarized in Table S1 (Supporting Information).[52–60]

2.3. Application Demonstrations of the TEWEH

A transparent sealed box with the TEWEH was placed in a wave tank to simulate the wave-driven operation and evaluate the output performance of the TEWEH. To verify the reliability of the TEWEH, we simulated harsh wave conditions on a wave tank and a six degrees of freedom platform, respectively. The specific layout and output details of TEWEH are shown in Figure S7 (Supporting Information). As shown in Video S2 (Supporting

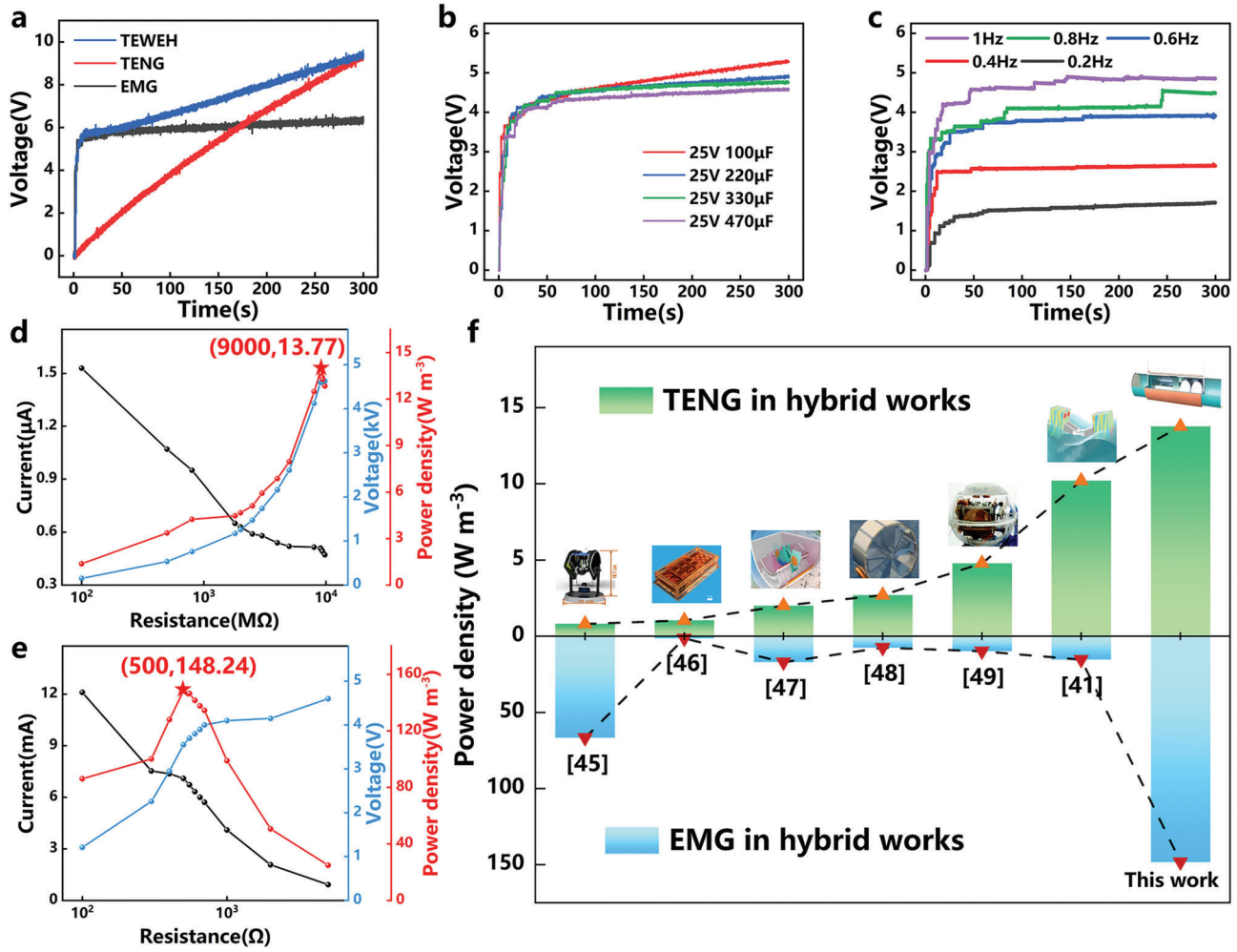

Figure 5. The electrical output performance of the TEWEH. a) Charging the 3.3 μF capacitor using the TENG component, the EMG component, and the TEWEH respectively. b) Charging various capacitors using the TEWEH. c) Charging the 330 μF capacitor using the TEWEH at different swinging frequencies. The power density of d) the TENG component and e) the EMG component. f) Comparison of the power density between this study and other hybrid wave energy harvesting studies. Images in (f) Reproduced with permission.[41–49] Copyright 2019, Wiley VCH, Copyright 2020, Elsevier, Copyright 2016, ACS, Copyright 2022, Wiley VCH, Copyright 2021, Elsevier, Copyright 2022, Elsevier.

Information), the TEWEH's output was stable (without leakage) under the harsh wave conditions on the six degrees of freedom platform. In addition, we found that the TEWEH maintained an excellent output after 10 800 cycles, as shown in Figure S8a,b (Supporting Information). The energy harvested by the TEWEH was stored in a capacitor through the rectifier circuit and subsequently converted into an appropriate output for various sensing devices via circuit management, as shown in **Figure 6**a. Navigation mark lights are electrical devices commonly used in marine environments. As shown in Figure 6b and Video S3 (Supporting Information), the TEWEH effortlessly lit the red (left) and green (right) navigation mark lights by charging a 330 μF capacitor. Similarly, as shown in Figure 6c and Video S4 (Supporting Information), the TEWEH was able to power a thermometer after a brief charge of a 330 μF capacitor. The capacitor charging and discharging diagram for powering the navigation mark lights and thermometer are shown in Figure S9a,b (Supporting Information), respectively.

Transmission of ocean information to receivers on land is important. To facilitate this, the TEWEH and the circuit module (CZJ-A1) were sealed in the same acrylic tube and deployed directly. The circuit module was equipped with a rectifier bridge, a 47 μF capacitor, a temperature sensor chip, and Bluetooth. The AC output from the TEWEH is rectified, and the resulting DC (direct current) power could charge the 47 μF capacitor. Once the voltage reached 5.2 V, temperature records were transmitted using Bluetooth. To ensure adequate buoyancy, the sealed tube containing the TEWEH and the circuit module was placed in a transparent sealed box. As shown in Figure S10 (Supporting Information), this is a simple and self-powered marine buoy. The testing site, as shown in Figure 6d, experienced a wind speed of ≈10 m s^{-1}. After swinging for ≈280 s, the module successfully established a connection with a mobile phone on land. The temperature was 26 °C initially, and 90 s later, the mobile phone updated the real-time ocean temperature to 14 °C. The demonstration is shown in Video S5 (Supporting Information). In an

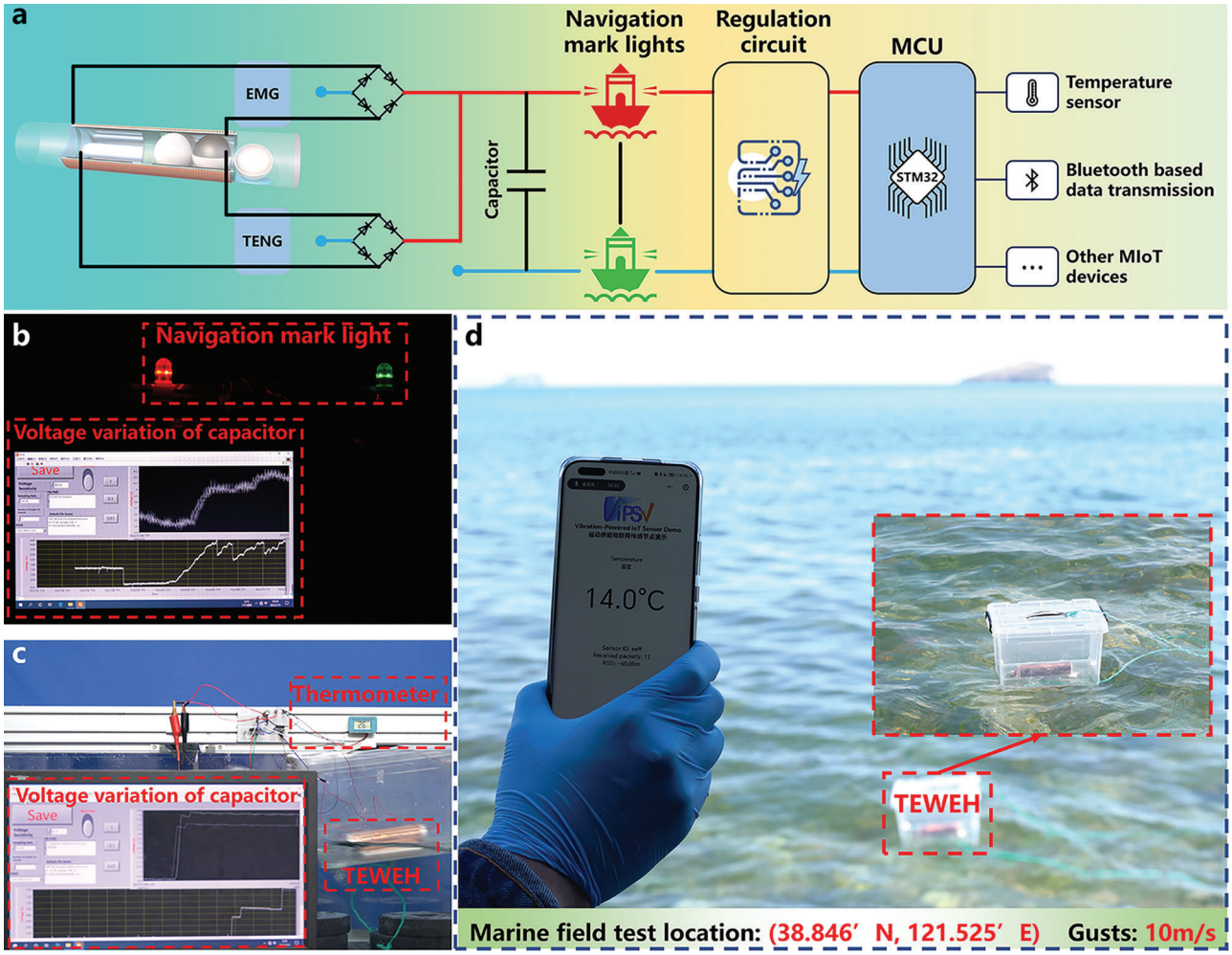

Figure 6. The application of the TEWEH. a) The schematic circuit diagram of the TEWEH as a power source for various sensing devices. b) The TEWEH lights up navigation mark lights. c) The TEWEH powers the thermometer. d) The TEWEH as a self-powered marine buoy deployed near Dalian Bay and transmits measurements to the receiver.

actual marine environment, the TEWEH has completed wave energy harvesting and wireless data transmission. Other data can be collected based on requirements, and the quantity and quality of data transmission can be improved by adding more TEWEH units.

3. Conclusion

In summary, a highly integrated tube-encapsulated triboelectric-electromagnetic wave energy harvester (TEWEH) toward self-powered marine buoy has been studied and demonstrated. The innovative material design of the PM-PTFE ball enabled the TENG to be highly integrated with the EMG, allowing both types of generators to operate simultaneously. The output performance of the TENG and EMG components was evaluated separately using horizontal and swinging experiments. Remarkably, the TEWEH demonstrated efficient wave energy harvesting capabilities even at low frequencies and amplitudes (angles). The swinging excitation yielded more desirable output results for the TEWEH, whereas the spherical motor design minimized the influence of the incident wave direction. The TEWEH can take advantage of the high voltage (230.25 V) of the TENG and high current (10.43 mA) of the EMG to charge the capacitors better and faster. The more prominent advantage is that the successful integration of the TENG and EMG components in the TEWEH resulted in a reduced device volume, enabling a higher power density. Specifically, the TENG component achieved an instantaneous power density of 13.77 W m^{-3}, while the EMG component reached 148.24 W m^{-3}. The output of the TEWEH is much higher than those of previously published hybrid structures, enabling it to provide direct power to navigation lights and some sensing devices easily after capacitor energy storage. In actual marine environments, the TEWEH achieved a significant milestone by successfully powering a Bluetooth temperature module and wirelessly transmitting real-time ocean temperature information to a receiver on land. However, there are still some challenges in the TEWEH coil layout, circuit management, and actual placement, which will be the next issue to address. In conclusion, if deployed

integrated with marine structures as a power network or independently as a self-powered marine buoy, the TEWEH exhibits tremendous potential for wave energy harvesting and self-powered MIoT.

4. Experimental Section

Fabrication of the TEWEH: A 25 mm diameter PM ball was embedded into a PTFE ball shell with an inner diameter of 25 mm and an outer diameter of 30 mm, forming a PM-PTFE ball. The TEWEH consists of a PM-PTFE ball and a PTFE ball (solid structure) with a mass of 72.09 g for the PM-PTFE and 30.11 g for the PTFE ball. The material of the PM ball was a NdFeB magnet (N48) because of its high magnetic field strength. To construct the device, both the PTFE and PM-PTFE balls were placed inside an acrylic tube with an inner diameter of 31 mm. Two 50 µm thick Al electrodes were affixed to the inner surface of the acrylic tube, with polished enamel-insulated wires connected as output terminals. There was a 1 cm gap between the electrodes. 0.3 mm diameter enamel-insulated wires were twisted around an acrylic tube (outer diameter of 35 mm) in three layers as a coil (≈1500 turns). The two ends of the acrylic tube were sealed using 2 mm thick acrylic plates with diameters of 35 mm. The entire device could be sealed with appropriately sized acrylic based on specific requirements.

Measurements and Statistical Analysis: The horizontal experiment system was driven by a linear motor (LinMot PS01-37X120F-HP-C), whereas the swinging experiment system was driven by a steering engine (Fashion Star HA8-U25). The TENG component's Q_{sc}, I_{sc}, and V_{oc} are measured using a precision impedance analyzer (Keithley 6514), whereas the output voltage and current of the EMG component were measured using a desktop multimeter (Keithley DMM6500). The remanence of the PM-PTFE ball was measured using a Gauss meter (TS500). The motion of the ball inside the tube is captured using a high-speed camera (Phantom v2012). The harsh wave conditions were simulated by a six degrees of freedom platform (TYSF-6-L450-300).

Supporting Information

Supporting Information is available from the Wiley Online Library or from the author.

Acknowledgements

C.Z., M.W., and C.L. contributed equally to this work. This work was supported by the National Key R & D Project from the Minister of Science and Technology (Grant No. 2021YFA1201604), the National Natural Science Foundation of China (Grant No. 52101382), Application Research Program of Liaoning Province (Grant No. 2022JH2/101300219), the China Postdoctoral Science Foundation (Fellowship No. 2022M710570), the Fundamental Research Funds for the Central Universities of China (Grant No. 3132023222/3132022221).

Conflict of Interest

The authors declare no conflict of interest.

Data Availability Statement

Research data are not shared.

Keywords

self-powered marine buoy, triboelectric-electromagnetic harvesters, wave energy

Received: May 31, 2023
Revised: July 21, 2023
Published online:

[1] R. Pelc, R. M. Fujita, *Mar. Policy* **2002**, *26*, 471.
[2] N. J. Murray, S. R. Phinn, M. DeWitt, R. Ferrari, R. Johnston, M. B. Lyons, N. Clinton, D. Thau, R. A. Fuller, *Nature* **2019**, *565*, 222.
[3] Y. Wen, P. Lin, *Energy Convers. Manag.* **2022**, *267*, 115901.
[4] Z. L. Wang, *Nature* **2017**, *542*, 159.
[5] B. Kamranzad, P. Lin, G. Iglesias, *Renew. Energy* **2021**, *172*, 697.
[6] S. H. Salter, *Nature* **1974**, *249*, 720.
[7] U. Henfridsson, V. Neimane, K. Strand, R. Kapper, H. Bernhoff, O. Danielsson, M. Leijon, J. Sundberg, K. Thorburn, E. Ericsson, K. Bergman, *Renew. Energy* **2007**, *32*, 2069.
[8] A. P. McCabe, A. Bradshaw, J. A. C. Meadowcroft, G. Aggidis, *Renew. Energy* **2006**, *31*, 141.
[9] K. Rhinefrank, E. B. Agamloh, A. Von Jouanne, A. K. Wallace, J. Prudell, K. Kimble, J. Aills, E. Schmidt, P. Chan, B. Sweeny, A. Schacher, *Renew. Energy* **2006**, *31*, 1279.
[10] Y. Zhang, Y. Zhao, W. Sun, J. Li, *Renew. Sustain. Energy Rev.* **2021**, *141*, 110764.
[11] R. Waters, M. Stålberg, O. Danielsson, O. Svensson, S. Gustafsson, E. Strömstedt, M. Eriksson, J. Sundberg, M. Leijon, *Appl. Phys. Lett.* **2007**, *90*, 034105.
[12] M. Wu, W. Guo, S. Dong, A. Liu, Y. Cao, Z. Xu, C. Lin, J. Zhang, *npj Mater. Degrad.* **2022**, *6*, 73.
[13] J. C. C. Henriques, J. C. C. Portillo, L. M. C. Gato, R. P. F. Gomes, D. N. Ferreira, A. F. O. Falcão, *Energy* **2016**, *112*, 852.
[14] Y. Li, Q. Guo, M. Huang, X. Ma, Z. Chen, H. Liu, L. Sun, *IEEE Access* **2019**, *7*, 129758.
[15] F. R. Fan, Z. Q. Tian, Z. L. Wang, *Nano Energy* **2012**, *1*, 328.
[16] Y. Wang, E. Yang, T. Chen, J. Wang, Z. Hu, J. Mi, X. Pan, M. Xu, *Nano Energy* **2020**, *78*, 105279.
[17] X. Li, Y. Cao, X. Yu, Y. Xu, Y. Yang, S. Liu, T. Cheng, Z. L. Wang, *Appl. Energy* **2022**, *306*, 117977.
[18] L. Zhang, B. Meng, Y. Tian, X. Meng, X. Lin, Y. He, C. Xing, H. Dai, L. Wang, *Nano Energy* **2022**, *95*, 107029.
[19] Z. Zhao, B. Wei, Y. Wang, X. Huang, B. Li, F. Lin, L. Ma, Q. Zhang, Y. Zou, F. Yang, H. Pang, J. Xu, X. Pan, *Nanomaterials* **2022**, *12*, 721.
[20] Z. Cao, Z. Yuan, C. Han, J. Feng, B. Wang, Z. L. Wang, Z. Wu, *ACS Appl. Nano Mater* **2022**, *5*, 11577.
[21] Y. Qi, Y. Kuang, Y. Liu, G. Liu, J. Zeng, J. Zhao, L. Wang, M. Zhu, C. Zhang, *Appl. Energy* **2022**, *327*, 120092.
[22] H. Yu, Z. Xi, Y. Zhang, R. Xu, C. Zhao, Y. Wang, X. Guo, Y. Huang, J. Mi, Y. Lin, T. Du, M. Xu, *Nano Energy* **2023**, *107*, 108182.
[23] W. Liu, L. Xu, G. Liu, H. Yang, T. Bu, X. Fu, S. Xu, C. Fang, C. Zhang, *iScience* **2020**, *23*, 101848.
[24] J. He, X. Fan, J. Mu, C. Wang, J. Qian, X. Li, X. Hou, W. Geng, X. Wang, X. Chou, *Energy* **2020**, *194*, 116871.
[25] X. Liang, Z. Liu, Y. Feng, J. Han, L. Li, J. An, P. Chen, T. Jiang, Z. L. Wang, *Nano Energy* **2021**, *83*, 105836.
[26] F. Xi, Y. Pang, G. Liu, S. Wang, W. Li, C. Zhang, Z. L. Wang, *Nano Energy* **2019**, *61*, 1.
[27] J. Feng, H. Zhou, Z. Cao, E. Zhang, S. Xu, W. Li, H. Yao, L. Wan, G. Liu, *Adv. Sci.* **2022**, *9*, 2204407.
[28] Y. Zi, H. Guo, Z. Wen, M. H. Yeh, C. Hu, Z. L. Wang, *ACS Nano* **2016**, *10*, 4797.
[29] Y. Hu, J. Yang, S. Niu, W. Wu, Z. L. Wang, *ACS Nano* **2014**, *8*, 7442.
[30] Y. Su, X. Wen, G. Zhu, J. Yang, J. Chen, P. Bai, Z. Wu, Y. Jiang, Z. L. Wang, *Nano Energy* **2014**, *9*, 186.
[31] S. Panda, S. Hajra, Y. Oh, W. Oh, J. Lee, H. Shin, V. Vivekananthan, Y. Yang, Y. K. Mishra, H. J. Kim, *Small* **2023**, *19*, 2300847.

[32] C. Rodrigues, M. Ramos, R. Esteves, J. Correia, D. Clemente, F. Gonçalves, N. Mathias, M. Gomes, J. Silva, C. Duarte, T. Morais, P. Rosa-Santos, F. Taveira-Pinto, A. Pereira, J. Ventura, *Nano Energy* **2021**, *84*, 105890.
[33] Z. Saadatnia, E. Asadi, H. Askari, E. Esmailzadeh, H. E. Naguib, *Int. J. Energy Res.* **2018**, *42*, 2431.
[34] X. Zhong, Y. Yang, X. Wang, Z. L. Wang, *Nano Energy* **2015**, *13*, 771.
[35] K. Zhang, X. Wang, Y. Yang, Z. L. Wang, *ACS Nano* **2015**, *9*, 3521.
[36] C. Hao, J. He, C. Zhai, W. Jia, L. Song, J. Cho, X. Chou, C. Xue, *Nano Energy* **2019**, *58*, 147.
[37] C. Wu, Q. Zhou, G. Wen, *Sensors Actuators, A Phys* **2021**, *326*, 112723.
[38] J. Ding, J. Jiang, T. Lin, G. Liu, H. Yao, H. Wen, S. Li, F. Mo, L. Wan, *Adv. Energy Sustain. Res.* **2022**, *3*, 2200087.
[39] J. Mu, H. He, J. Song, J. He, X. Hou, X. Han, C. Feng, J. Zou, J. Yu, X. Chou, *Energy Reports* **2022**, *8*, 5272.
[40] Y. Luo, P. Chen, L. N. Y. Cao, Z. Xu, Y. Wu, G. He, T. Jiang, Z. L. Wang, *Adv. Funct. Mater.* **2022**, *32*, 2205710.
[41] J. Wang, L. Pan, H. Guo, B. Zhang, R. Zhang, Z. Wu, C. Wu, L. Yang, R. Liao, Z. L. Wang, *Adv. Energy Mater.* **2019**, *9*, 1802892.
[42] Y. Wang, Z. Qian, C. Zhao, Y. Wang, K. Jiang, J. Wang, Z. Meng, F. Li, C. Zhu, P. Chen, H. Wang, M. Xu, *Adv. Mater. Technol.* **2023**, *8*, 2201245.
[43] X. Sun, C. Shang, H. Ma, C. Li, L. Xue, Q. Xu, Z. Wei, W. Li, Y. Yalikun, Y. C. Lai, Y. Yang, *Nano Energy* **2022**, *100*, 107540.
[44] W. J. Kim, V. Vivekananthan, G. Khandelwal, A. Chandrasekhar, S. J. Kim, *ACS Appl. Electron. Mater.* **2020**, *2*, 3100.
[45] X. Chen, L. Gao, J. Chen, S. Lu, H. Zhou, T. Wang, A. Wang, Z. Zhang, S. Guo, X. Mu, Z. L. Wang, Y. Yang, *Nano Energy* **2020**, *69*, 104440.
[46] X. Wang, Z. Wen, H. Guo, C. Wu, X. He, L. Lin, X. Cao, Z. L. Wang, *ACS Nano* **2016**, *10*, 11369.
[47] C. Han, Z. Cao, Z. Yuan, Z. Zhang, X. Huo, L. Zhang, Z. Wu, Z. L. Wang, *Adv. Funct. Mater.* **2022**, *32*, 2205011.
[48] Y. Feng, X. Liang, J. An, T. Jiang, Z. L. Wang, *Nano Energy* **2021**, *81*, 105625.
[49] H. Hong, X. Yang, H. Cui, D. Zheng, H. Wen, R. Huang, L. Liu, J. Duan, Q. Tang, *Energy Environ. Sci.* **2022**, *15*, 621.
[50] T. Zhao, M. Xu, X. Xiao, Y. Ma, Z. Li, Z. L. Wang, *Nano Energy* **2021**, *88*, 106199.
[51] H. Wang, C. Zhu, W. Wang, R. Xu, P. Chen, T. Du, T. Xue, Z. Wang, M. Xu, *Nanomaterials* **2022**, *12*, 594.
[52] R. Ouyang, Y. Huang, H. Ye, Z. Zhang, H. Xue, *Nano Energy* **2022**, *102*, 107749.
[53] Q. Zhang, M. He, X. Pan, D. Huang, H. Long, M. Jia, Z. Zhao, C. Zhang, M. Xu, S. Li, *Nano Energy* **2022**, *103*, 107810.
[54] H. Jung, H. Ouro-Koura, A. Salalila, M. Salalila, Z. D. Deng, *Nano Energy* **2022**, *99*, 107365.
[55] W. Ding, B. Song, Z. Mao, K. Wang, *J. Mar. Sci. Technol.* **2016**, *21*, 359.
[56] S. Chen, B. Jiang, X. Li, J. Huang, X. Wu, Q. Xiong, R. G. Parker, L. Zuo, *Appl. Energy* **2022**, *321*, 119320.
[57] W. Chen, Y. Lu, S. Li, F. Gao, *Appl. Energy* **2023**, *334*, 120696.
[58] Y. Zhang, Y. Wen, X. Han, W. Zhang, F. Gao, W. Chen, *Ocean Eng* **2023**, *273*, 113819.
[59] W. Chen, X. Lin, Y. Lu, S. Li, L. Wang, Y. Zhang, F. Gao, *Renew. Energy* **2023**, *202*, 1497.
[60] A. Ahmed, Y. Wang, A. Azam, N. Li, C. Jia, Z. Zhang, *Ocean Eng* **2023**, *275*, 114162.